Manganese as a structural promoter in silica-supported cobalt Fischer-Tropsch catalysts under simulated high conversion conditions

van Koppen, Luke M.; Dugulan, A.I.; Leendert Bezemer, G.; Hensen, Emiel J.M.

Important note
To cite this publication, please use the final published version (if applicable).
Please check the document version above.

Manganese as a structural promoter in silica-supported cobalt Fischer-Tropsch catalysts under simulated high conversion conditions

Luke M. van Koppen [a,b], A. Iulian Dugulan [b], G. Leendert Bezemer [c], Emiel J.M. Hensen [a,*]

[a] Laboratory of Inorganic Materials and Catalysis, Department of Chemical Engineering and Chemistry, Eindhoven University of Technology, Het Kranenveld 14, 5600 MB Eindhoven, The Netherlands
[b] Laboratory of Fundamentals Aspects of Materials and Energy, Department of Radiation Science & Technology, Delft University of Technology, Mekelweg 15, 2628 CD Delft, The Netherlands
[c] Energy Transition Campus Amsterdam, Shell Global Solutions International B.V., Grasweg 31, 1031 HW Amsterdam, The Netherlands

ARTICLE INFO

ABSTRACT

Understanding the deactivation mechanism of cobalt-based Fischer-Tropsch catalysts is of significant practical importance. Herein, we explored the role of manganese as a structural promoter on silica-supported cobalt nanoparticles under simulated high CO conversion conditions, i.e., high relative humidity. The structural changes in cobalt dispersion and oxidation state were followed by *in situ* Mössbauer emission spectroscopy. Adding manganese oxide to silica-supported cobalt enhanced the dispersion of metallic cobalt in the reduced catalysts. This higher cobalt dispersion, however, led to a stronger tendency of cobalt silicate formation under humid conditions. Without manganese, the cobalt particles sintered, and the larger ones were prone to transformation into cobalt carbide under high conversion conditions. As such, silica is not preferred as a support for practical FTS.

1. Introduction

Fischer-Tropsch synthesis (FTS) is a surface-catalyzed polymerization reaction that converts a feed of synthesis gas (CO + H₂) to fuels and chemicals [1]. The current commercial exploitation of this technology mainly utilizes cobalt catalysts to convert synthesis gas derived from natural gas into primarily long-chain paraffins [2]. FTS also holds promise to convert feedstocks from renewable sources, such as biomass, which is crucial to the energy transition in which our dependence on fossil resources needs to decrease. Since cobalt-based FTS is dictated by a strong particle size effect, catalyst design is essential with an optimum size of cobalt nanoparticles around 6–8 nm [3,4]. An important aspect of practical FTS is catalyst stability, which is broadly investigated [5].

Two dominant deactivation profiles can be discerned in cobalt-based FTS [6]. Short-term deactivation is well studied [5,7,8] and is the result of wax condensation and resulting diffusion limitations, which can typically be reversed by a mild hydrogen treatment [9]. Long-term deactivation, on the other hand, is often the result of structural changes in the catalyst and is typically less reversible, making it significant in industrial practice. Long-term deactivation is poorly understood, with several factors contributing to the loss of catalytic activity

over time. The most common ones are oxidation of the active metal phase [10–13], strong-metal support interactions (SMSI) [14–16], carbon deposition [17–19], and cobalt sintering [20–22].

In the study of deactivation, the support plays an important role. Such studies employ model carbon support [4,23,24] or, of more practical relevance, oxide supports such as SiO₂ [16,25,26], Al₂O₃ [2,27,28], and TiO₂ [29–32]. Carbon is a support with weak interaction with cobalt, an excellent model system for studying sintering and other deactivation mechanisms [24]. In industrial applications, oxide supports are used, because the stronger interactions with cobalt lead to a better stability of the active phase. And it allows for catalyst regeneration through an oxidation and reduction cycle [8]. The interaction between cobalt and the support can also result in the formation of cobalt-support compounds [33,34], which can also lead to significant irreversible deactivation, especially in the presence of steam [35,36].

Water is a main product of the FTS reaction, because the main pathway for O removal from the surface upon CO dissociation is through the production of water. High partial pressures of steam (humidity) can facilitate cobalt deactivation through oxidation, SMSI, carbide formation [24], or sintering. Thermodynamics dictate that spherical cobalt nanoparticles smaller than about 4 nm oxidize at relevant H₂O/H₂ ratios

---

during FTS conditions [11]. However, bulk oxidation of supported cobalt catalysts under (simulated) industrial FTS conditions is often not observed, which can be because typical catalysts contain larger particles or due to kinetic limitations of water dissociation in simulated conditions, when tests are done in the absence of CO [5,10,13,37,38]. The effect of steam on sintering under FTS conditions has also been investigated [21,24,38]. The combination of high partial pressure of steam and carbon monoxide accelerates agglomeration of the active metal phase. The exact mechanisms at play are still a matter of discussion. Kliewer et al. proposed that surface wetting by cobalt oxide/hydroxide species facilitates interaction between neighbouring metallic particles, resulting in coalescence [31]. A narrow particle size distribution, well separated on the support, is essential to resist steam-induced sintering. On the other hand, Moodley et al. explained cobalt sintering by Ostwald ripening involving sub-carbonyl species as the dominant mechanism, which is also enhanced by the presence of water [7].

High coverage of the support by carbon deposits can also result in structural changes in the catalyst, and the formation of cobalt carbides has been reported [39]. While iron carbide is the active phase in iron-based catalysts, the formation of cobalt carbide is undesired as it presents a much lower activity than metallic cobalt and has a much lower selectivity towards heavy paraffins [40–42]. Thermodynamics show that cobalt carbides are stable under FTS conditions, implying their formation is kinetically hindered [39].

Manganese oxide has been investigated as a constituent of cobalt-based FTS catalysts already in the first half of the 20th century [43]. These early results showed the potential of manganese to reduce methane selectivity. Later, pioneering studies using catalysts prepared by co-precipitation of cobalt and manganese led to a better understanding of the role of manganese oxide as a support and selectivity promoter [44–47]. More recently, the focus has been on manganese oxide as a promoter for supported cobalt FTS catalysts [23,48–50], in which a positive impact on the chain-growth probability has been emphasized. However, concurrent work by Kimpel et al. [51] has shown that the C_{5+} selectivity is only improved by manganese promotion at low operating pressures. Adding manganese leads to a lower chain-growth probability at high operating pressures (i.e., 10–30 bar). Contrary to their work, we focus on the structural effects of manganese promotion and whether it can improve catalyst stability under high conversion conditions. In our previous study, we looked at manganese promotion on a carbon-supported system [24] and observed cobalt carbide formation under industrial operating conditions. This formation was a direct result of the high mobility of both cobalt and manganese oxide under reaction conditions on the weakly interacting CNF support. And so, in the present work, we again focus on the role of manganese oxide as a structural promoter but on a stronger interacting oxidic support, namely silica. Structural deactivation is investigated under FTS reaction conditions at elevated pressure by *in situ* Mössbauer emission spectroscopy (MES) [52]. The effect of water partial pressure on the deactivation is studied by feeding steam to the reactor to reach industrially relevant bottom bed conditions. Previous ^{57}Co MES studies showed that these high pressures of water increase cobalt sintering [24,38] and can result in oxidation as well as strong-metal support interactions [36,53]. The current MES measurements are supplemented by *quasi in situ* XPS, TEM, and XRD characterization, while the catalytic performance is measured *in situ* and a microflow reactor.

2. Experimental methods

2.1. Catalyst preparation

All supported catalysts were prepared by incipient wetness impregnation of X080 silica extrudates (Shell Global Solutions International B. V., pore volume 0.84 mL/g) followed by drying in air at 120 °C for 6 h. The impregnation solutions were obtained by dissolving the appropriate amount of $Co(NO_3)_2 \cdot 6H_2O$ (≥98.0 %, Sigma Aldrich) and Mn

$(NO_3)_2 \cdot 3H_2O$ (≥97.0 %, Sigma Aldrich) in dehydrated ethanol, and mixing with a solution of $Pt(NH_3)_4(NO_3)_2$ (≥99.995 %, Sigma Aldrich) in de-ionized water to form a homogenous mixture. Three catalysts were prepared with a cobalt loading of 8 wt%, 0.08 wt% platinum, and 0, 0.8, and 1.6 wt% manganese, respectively. The resulting samples are denoted by CoMn(x)Pt/SiO$_2$, where x represents the intended manganese to cobalt ratio. Following impregnation and drying, the samples were calcined at 350 °C for 2 h in stagnant air (rate 5 °C/min). Part of these calcined catalysts was spiked with radioactive ^{57}Co by pore volume impregnation using a solution containing 90 MBq ^{57}Co in 0.1 M HNO$_3$. These radioactive samples were dried at 120 °C for 12 h and used for Mössbauer spectroscopy.

2.2. Characterization

2.2.1. X-ray diffraction

X-ray diffraction (XRD) patterns were recorded on a Bruker D2 Phaser using a Cu Kα radiation source and a 2 mm slit. Data was collected using a time per step of 0.15 min and a step size of 0.1° in the 2θ range of 10–65°. Background subtractions were applied, and reference spectra were obtained using the Diffrac.Eva software by Bruker.

2.2.2. Quasi in situ X-ray photoelectron spectroscopy

The oxidation state and cobalt dispersion were studied by *quasi in situ* XPS using a Kratos AXIS Ultra 600 spectrometer equipped with a monochromatic Al Kα X-ray source (Al Kα 1486.6 eV). Survey scans were recorded at a pass energy of 160 eV and detailed region scans at 40 eV. The step size was 0.1 eV, and the background pressure during the measurements was kept below 10^{-9} mbar.

A high-temperature reaction cell (Kratos, WX-530) was used to pretreat the sample supported on an alumina stub, allowing *in vacuo* sample transfer into the analysis chamber. Reduction was performed in a pure H$_2$ flow at atmospheric pressure and 350 °C for 2 h. After reduction, the reaction cell was evacuated to a pressure below 10^{-9} mbar. Then, the sample was cooled to 150 °C and transferred to the analysis chamber. Data analysis was done with the CasaXPS software (version 2.3.22PR1.0). The binding energy scale was corrected for surface charging by taking the C 1s peak of adventitious carbon as a reference at 284.8 eV.

The degree of reduction (DOR) is calculated by comparing the peak areas corresponding to the fitted metallic and oxidic cobalt contributions using a model described by Biesinger et al. [54]. The Co/Si ratio is determined using a survey scan and comparing the peak areas of the Co 2p and Si 2p contributions.

2.2.3. Electron microscopy

Surface averaged particle sizes and particle size distributions were determined using transmission electron microscopy (TEM). TEM measurements were performed on an FEI Tecnai 20 electron microscope operated at an electron acceleration voltage of 200 kV with a LaB6 filament. Typically, a small amount of the sample was ground and suspended in pure ethanol, sonicated, and dispersed over a Cu grid with a holey carbon film.

2.2.4. In situ Mössbauer emission spectroscopy

Mössbauer emission spectroscopy (MES) was carried out at various temperatures using a constant acceleration spectrometer set up in a triangular mode with a moving single-line K$_4$Fe(CN)$_6 \cdot 3H_2O$ absorber enriched in ^{57}Fe. The velocity scale was calibrated with a ^{57}Co:Rh source and a sodium nitroprusside absorber. Zero velocity corresponds to the peak position of the K$_4$Fe(CN)$_6 \cdot 3H_2O$ absorber measured with the ^{57}Co: Rh source, positive velocities correspond to the absorber moving towards the source. A high-pressure MES cell is used to measure under *in situ* Fischer-Tropsch conditions [52], described in detail in the literature [24].

Mössbauer spectra were fitted using the MossWinn 4.0 program [55].

The spectra of very small superparamagnetic species were fitted using the two-state magnetic relaxation model of Blume and Tjon, which assumes the presence of a fluctuating magnetic field that jumps between the values of +H and −H along the z-axis with an average frequency τ [56]. H typically equals 500 kOe, and τ can vary between 10^{-9} and 10^{-12} s^{-1}. The Mössbauer spectra of larger particles were fitted using a hyperfine sextuplet, resulting from the local magnetic field experienced by bulk metallic particles. The experimental uncertainties in the calculated Mössbauer parameters, estimated using Monte Carlo iterations by the MossWinn 4.0 program and including experimental uncertainties, were as follows: IS and QS ± 0.01 mm s^{-1} for the isomer shift and quadrupole splitting, respectively; ±3 % for the spectral contribution; ±3 kOe for the hyperfine field.

Typically, 300 mg of radioactivity-spiked and 100 mg of non-radioactive catalyst (sieve fraction 250–500 μm) were loaded into two separate compartments of the reactor cell. FTS experiments were performed *in situ* following reduction at 350 °C for 2 h in 100 mL/min. flow of pure H$_2$. Reactions were done at 200 °C and 20 bar, while the CO/H$_2$ was kept at 4 throughout, and steam was fed to vary the relative humidity. Water was evaporated and mixed with the incoming feed gas using a controlled evaporator mixer (CEM, Bronkhorst). Wax products were collected in a downstream hot catch pot, and water was retrieved in a subsequent cold catch pot. An online Trace GC Ultra from Thermo Fisher Scientific (RT-Silica bond column and a flame ionization detector, a Stabilwax column and a thermal conductivity detector) was used to analyze the gaseous products.

2.3. Catalytic activity measurements

The catalytic performance was determined in a single-pass flow reactor system (Microactivity Reference unit, PID Eng&Tech) operated at a temperature of 220 °C or 240 °C, a total pressure of 20 bar, and an H$_2$/CO ratio of 4. In a typical experiment, 50 mg of catalyst (sieve fraction 125–250 μm) mixed with SiC particles of the same sieve fraction to a total volume of 3 mL was placed in a tubular reactor with an internal diameter of 9 mm. The temperature was controlled via a thermocouple in the center of the catalytic bed. Reduction was first performed in a flow of H$_2$ at 350 °C for 2 h after heating at a rate of 5 °C/min. Subsequently, the reactor was cooled to 220 °C, and the gas feed composition was changed to reaction conditions. A space velocity (SV) of 60 L g$_{cath}^{-1}$h^{-1}, was applied, which resulted in a CO conversion of approximately 5 %. A TRACE1300 GC instrument (Thermo Fisher Scientific) equipped with two columns (a RT-Silica bond column and a flame ionization detector, a Porabond-Q column, and a thermal conductivity detector) was used to measure the gas composition of the reactor effluent. The Weisz−Prater criterion was calculated to confirm the reactions did not run under internal mass transfer limitations. At the applied reaction conditions, no CO$_2$ was observed, and the selectivity toward oxygenates on a molar carbon basis was less than 1 %. Liquid products and waxes were collected in a cold trap after the reactor. Ar was used an internal standard in the CO/H$_2$ feed mixture. The CO conversion (X$_{CO}$) was determined in the following manner:

$$X_{CO} = 1 - \frac{n_{Ar,in}n_{CO,out}}{n_{CO,in}n_{Ar,out}} \tag{1}$$

where $n_{Ar,in}$ is the molar Ar flow in the reactor feed, $n_{CO,in}$ is the molar CO flow in the reactor feed, and $n_{Ar,out}$ and $n_{CO,out}$ are the respective molar flows of Ar and CO out of the reactor system.

The carbon-based selectivity of hydrocarbon compound C$_i$ (S$_{Ci}$) was calculated using:

$$S_{Ci} = \frac{n_{Ar,in}n_{Ci}v_i}{n_{Ar,out}n_{CO,in}X_{CO}} \tag{2}$$

where n_{Ci} is the molar flow of hydrocarbon compound C$_i$ out of the reactor, and v_i is the stochiometric factor of the hydrocarbon compound.

The cobalt time-yield (CTY) was determined using the following equation:

$$CTY = \frac{F_{CO,in}X_{CO}}{m_{Co}} \tag{3}$$

where m$_{Co}$ is the weight of cobalt loaded in the reactor.

The turnover frequency (TOF) was calculated using the following equation:

$$TOF = \frac{CTYMw_{Co}}{D} \tag{4}$$

where Mw$_{Co}$ is the atomic weight of cobalt, and D the dispersion of cobalt. The dispersion is calculated as follows:

$$D = 6\frac{(V_{Co}/a_{Co})}{d_p} \tag{5}$$

where v_{Co} is the volume occupied by a cobalt atom in the bulk, a_{Co} the surface area occupied by an atom of cobalt on the surface, and d_p is the average cobalt particle size.

3. Results and discussion

3.1. Fresh catalyst characterization

Fig. 1 shows representative TEM images of the catalysts after calcination at 350 °C for 2 h in stagnant air. The average size and size distribution of the cobalt oxide nanoparticles were determined by analyzing approximately 150 particles in ca. eight images per sample. The average particle sizes are given in Table 1. The particle size distribution of the calcined catalysts is not significantly affected by the presence of manganese. However, the data can hint at a slight decrease in the particle size with increasing manganese content.

The X-ray diffractograms of the calcined catalysts are given in Fig. 2. All samples show the expected broad diffuse scattering feature of the amorphous silica support and the diffraction lines of cobalt oxide (Co$_3$O$_4$). Although manganese oxides have no diffraction features in the manganese-containing samples, a slight broadening of the main cobalt oxide diffraction line is observed, which may hint at a smaller size of the cobalt oxide phase. The FWHM of the diffraction line at 36.8°CoPt/SiO$_2$ is smaller (0.76°) than that of CoMn(0.2)Pt/SiO$_2$ (1.06°). By applying the Scherrer equation and assuming a shape factor of 0.9 [57], cobalt oxide crystallite sizes of 11.0 nm for the non-promoted samples and 7.9 nm for the promoted sample are determined. The TEM values are significantly lower, which is reasonable as XRD does not probe small cobalt oxide nanoparticles. Nevertheless, these results show that the presence of manganese leads to an increased cobalt dispersion in the oxidic precursor.

We then analysed the calcined and reduced state of the various catalysts by XPS. The cobalt spectra are given in Fig. 3. Fitting of the Co 2p spectra was done using the model of Biesinger et al. [54]. The degree of reduction (DOR) upon reduction at 350 °C in pure hydrogen was determined from the metallic cobalt contribution to the Co 2p$_{3/2}$ spectra. The non-promoted and promoted catalysts display a high DOR (Table 1). Table 1 also shows the Co/Si ratios before and after reduction. The finding that this ratio is nearly the same before and after reduction suggests that the reduction treatment does not lead to extensive sintering. This is likely the result of the interactions between the silica support and cobalt, which differs from the extensive sintering seen for cobalt on titania [53,58]. Comparison of the Co/Si ratios of CoPt/SiO$_2$ and CoMn (0.2)Pt/SiO$_2$ shows that manganese promotion leads to a higher cobalt dispersion in the oxidic precursor, which is maintained upon reduction. These findings agree with the TEM and XRD results, which also emphasized the positive effect of manganese on cobalt dispersion in the calcined catalyst. The Mn 2p XPS spectra before and after reduction are given in Fig. S5. The Mn signal for the promoted catalysts in the calcined
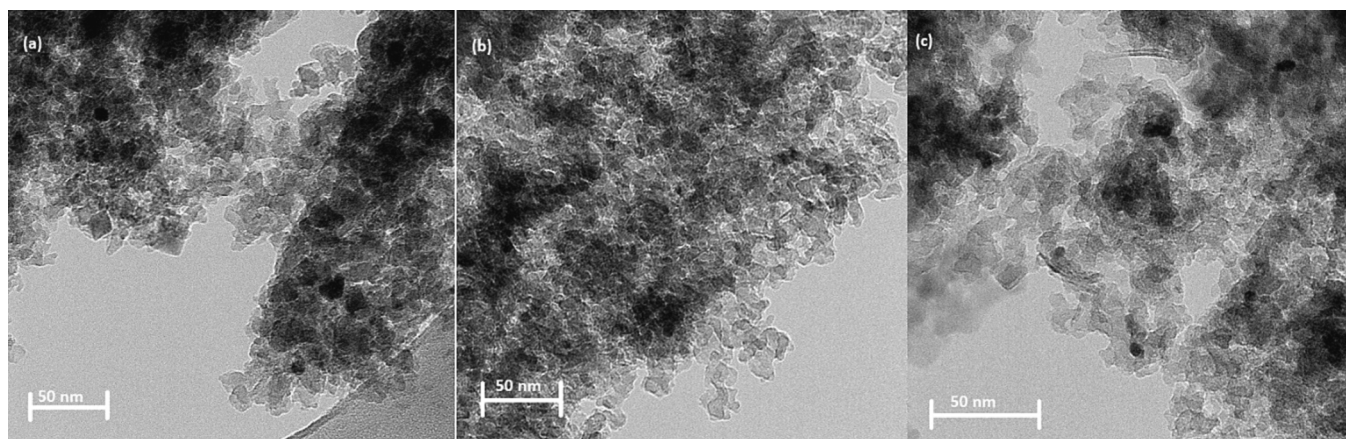
Fig. 1. Representative TEM images of (a) CoPt/SiO$_2$, (b) CoMn(0.1)Pt/SiO$_2$, and (c) CoMn(0.2)Pt/SiO$_2$ following calcination at 350 °C for 2 in stagnant air.

Table 1
Average metal oxide particle size, Co/Si ratio, and Co(Mn)Pt/SiO2 catalyst reducibility.

Catalyst	Particle size (nm)[a]	Co/Si[b] (calcined)	Co/Si[b] (reduced)	DOR (%)[c]
CoPt/SiO$_2$	6.1 ± 3.8	0.16	0.15	73
CoMn(0.1)Pt/ SiO$_2$	5.4 ± 2.6	0.21	–	–
CoMn(0.2)Pt/ SiO$_2$	5.2 ± 2.4	0.29	0.28	79

[a] Determined by TEM analysis of calcined samples, [b] Atomic Co/Si ratio determined by XPS, [c] Degree of reduction determined by XPS.

state was very weak. After reduction, clear Mn^{2+} contributions are observed for the CoMn(0.2)Pt/SiO$_2$ sample. This suggests that the reduction treatment resulted in an improved manganese dispersion, which has been earlier observed by Weckhuysen et al. [59] and was attributed to the migration of manganese towards the support upon reduction of mixed oxide particles. However, the formation of MnO on the surface of metallic cobalt can also contribute to the improved signal-to-noise ratio.

3.2. In situ Mössbauer emission spectroscopy reduced catalysts

Mössbauer spectra of catalysts reduced in hydrogen at 350 °C for 2 h are given in Fig. 4. The elevated noise observed on the CoMn(0.1)Pt/ SiO$_2$ comes from the radioactive probe, which had decreased activity due to its natural decay. Which resulted in fewer counts over the
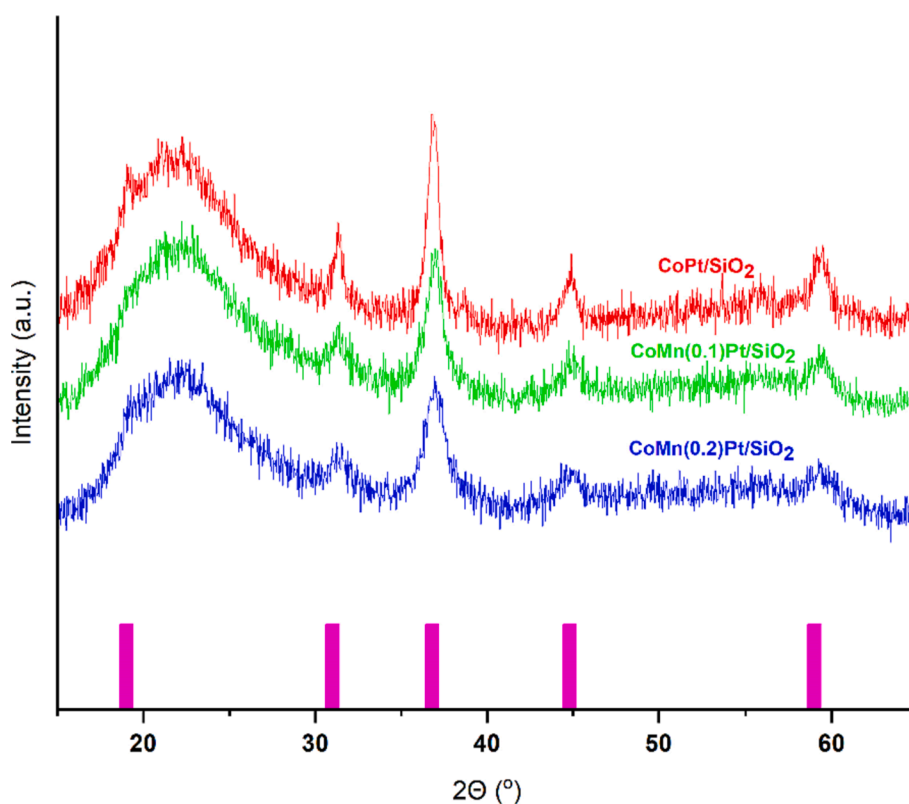

Fig. 2. X-ray diffractograms of as-prepared CoMn(0.2)Pt/SiO$_2$ (blue), CoMn(0.1)Pt/SiO$_2$ (green), and CoPt/SiO$_2$ (red) following calcination at 350 °C (main Co$_3$O$_4$ reflections in magenta). (For interpretation of the references to colour in this figure legend, the reader is referred to the web version of this article.)
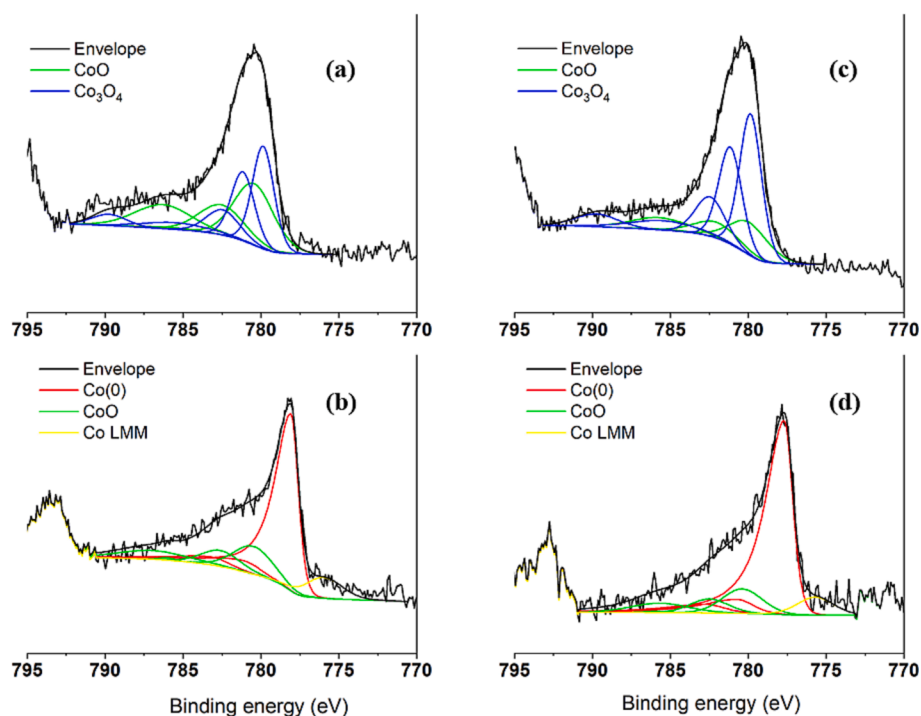
Fig. 3. XPS spectra of CoPt/SiO$_2$ (a,b) and CoMn(0.2)Pt/SiO$_2$ (c,d) after (a,c) calcination and (b,d) subsequent reduction at 350 °C (black: experimental data and the fitted envelope; red: the fitted metallic Co(0) contributions; green: the fitted CoO contributions; blue: fitted Co$_3$O$_4$ contributions; yellow: the Co auger LMM peak; the XPS fit model was taken from Ref. [54]). (For interpretation of the references to colour in this figure legend, the reader is referred to the web version of this article.)

constant measurement time. The spectra contain two main contributions: a sextuplet with an isomer shift (IS) of −0.1 mm s-1 and a hyperfine field (HF) between 310 and 317 kOe, and a singlet with an IS of 0.0 mm s^{-1}. Both these features are related to metallic cobalt. The sextuplet represents a contribution of magnetically ordered cobalt metal particles, common when their size is larger than 6 nm [38]. The observed singlet indicates that the reduced catalyst contains small superparamagnetic metallic particles without magnetic ordering, typical for particles smaller than 6 nm. The observation of significant contributions of both phases indicates that the reduced samples contain particles with sizes around the SPM cut-off of 6 nm. Compared to CoPt/SiO$_2$, the manganese-containing samples contain a significantly higher contribution of SPM cobalt. Additionally, the measured HF of the two manganese-promoted catalysts is considerably lower (310–311 kOe) than for the non-promoted catalyst (317 kOe). As the HF also correlates to the domain size of magnetically ordered cobalt, these differences point to smaller particles in the presence of manganese. Both these observations indicate a higher cobalt dispersion after reduction when manganese is present as a promoter. It is important to note that the MES spectra do not contain evidence of doublets due to cobalt oxide, which implies a high cobalt reduction degree.

3.3. In situ Mössbauer emission spectroscopy during the FTS reaction

In situ Mössbauer spectra were recorded for the catalysts as a function of the steam partial pressure at a temperature of 200 °C, a total pressure of 20 bar, and a H$_2$/CO ratio of 4. The steam content in the feed is expressed as the relative humidity (RH) at the applied conditions. Table S1 details the feed compositions for the different experiments. Spectra were recorded for at least 48 h at each humidity step, except for RHs of 25 % and 57 %, where the steam treatment was prolonged to 5 days and 11 days, respectively. This was done to understand the influence of prolonged exposure in industrial practice.

Under relatively low humidity conditions up to RH = 25 %, only minor changes are observed in the Mössbauer spectra (Fig. 5a). The

spectral contribution of the SPM phase did not decrease significantly for the promoted and non-promoted samples, as can be deduced from Table 2. The absence of a decreasing SPM metallic cobalt contribution indicates that significant sintering of the small metallic cobalt particles does not occur under these conditions.

When the humidity is further increased to RH = 57 %, two new phases are observed in the Mössbauer spectra (Fig. 5b). For CoPt/SiO$_2$, a Co$_2$C phase with a spectral contribution of 13 % is present. This phase is characterized by an isomer shift (IS) of 0.0 mm s^{-1} and a quadrupole splitting (QS) of 0.9 mm s^{-1}, as also reported for cobalt carbide formed in a carbon-supported cobalt catalyst [24]. The other phase appearing is a Co^{2+}-containing phase with a spectral contribution of 4 %. This feature is also observed in both promoted catalysts but with a significantly higher spectral contribution. The assignment of this doublet with an IS of 0.9 mm s^{-1} and a QS of 1.8 mm s^{-1} is based on the similarity of the Mössbauer parameters to previously observed Fe^{2+}-doublets in ferrosilicate (FeSiO$_3$) materials [60]. As such, this points towards forming metal-support compounds (MSC) under high humidity conditions. Unlike CoPt/SiO$_2$, exposing the manganese-promoted catalysts to the highest RH did not lead to the formation of cobalt carbide. This contrasts the formation of cobalt carbide in a manganese-promoted cobalt FTS catalyst supported on carbon nanofibers [24]. In the carbon-supported case, cobalt carbide formation was linked to cobalt being in close contact with larger manganese oxide agglomerates. The absence of cobalt carbide in the silica-supported samples containing manganese can be rationalized by the stronger metal-support interactions that decrease the mobility of cobalt and manganese. The formation of cobalt carbide in the non-promoted catalyst under high humidity conditions is likely the result of the increased CO partial pressure under these conditions. However, the high partial pressures of steam can also affect the phases present, as a previous study showed an increasing amount of cobalt carbide under *in situ* FTS conditions on an alumina support with increasing water partial pressure [39]. Another study of cobalt on alumina showed the importance of the metallic cobalt particle size, with larger cobalt particles (10–11 nm) being susceptible to carbidization
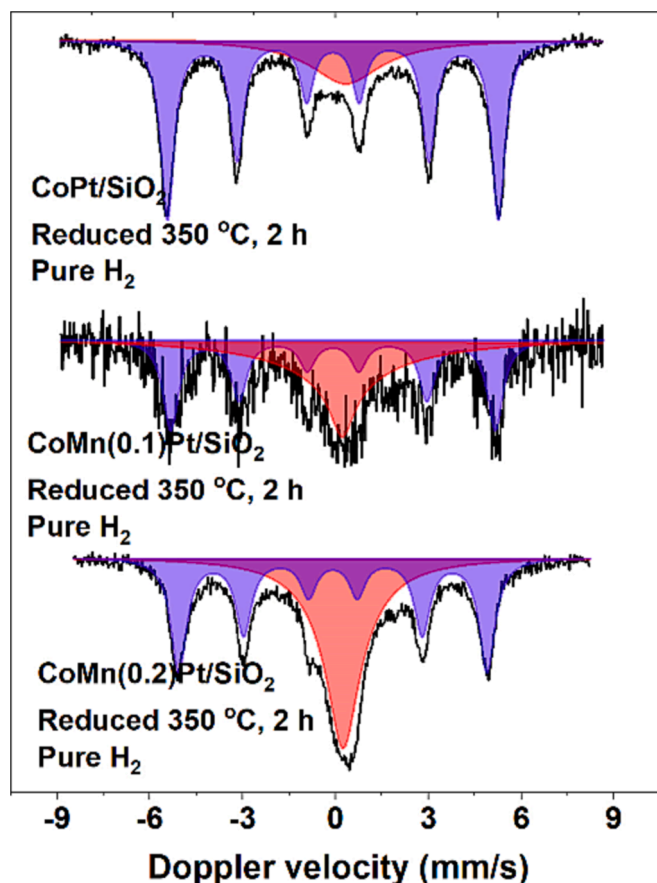
Fig. 4. Mössbauer spectra of Co(Mn)Pt/SiO$_2$ catalysts after reduction at 350 °C in pure hydrogen: black lines represent the experimental spectra, blue the fitted bulk metallic cobalt, and red the fitted SPM metallic cobalt singlet. (For interpretation of the references to colour in this figure legend, the reader is referred to the web version of this article.)

under FTS conditions in contrast to smaller ones (6 nm) [37]. This observation agrees with our MES results which showed that the final reduction transformed carbide into a bulk sextuplet with the highest associated HF in this study, indicative of the largest cobalt particles. Such an effect of particle size on carbidization can explain why cobalt carbide formation was not observed for the manganese-promoted samples in the present study, as their metallic particles were significantly smaller. Thermodynamic calculations point towards the stability of cobalt carbide (Co$_2$C) under FTS conditions [39,61]. This suggests that its formation under FTS conditions is strongly kinetically inhibited.

As previously discussed, the ratio of the SPM and magnetically ordered cobalt contributions is higher for the two manganese-promoted catalysts than their non-promoted counterparts. Following the high humidity treatment, these catalysts show a much higher spectral contribution of a cobalt-silicate phase, namely 33 % for the CoMn(0.1) Pt/SiO$_2$ catalyst, and 24 % for the CoMn(0.2)Pt/SiO$_2$ sample. As the catalyst with a lower manganese loading shows a higher spectral contribution of the MSC, it is unlikely that cobalt-silicate formation is directly facilitated by manganese oxide. Instead, it is reasonable to consider that the more significant contribution of small metallic SPM cobalt particles causes the formation of more cobalt-silicate. It has been

Table 2
Contribution of SPM metallic cobalt obtained from Mössbauer spectra measured at 200 °C, 20 bar pressure, H$_2$/CO = 4 as a function of the relative humidity.

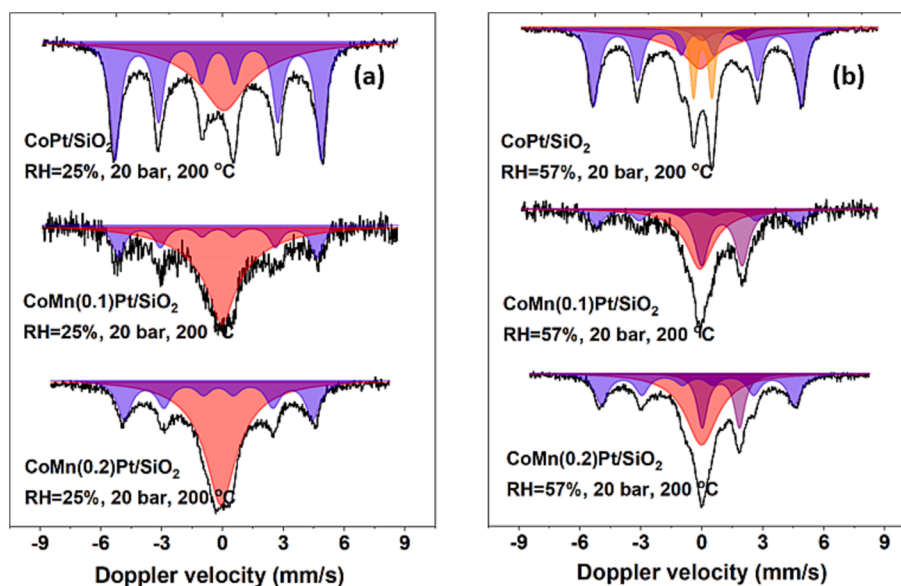| Treatment relative humidity (%)	H$_2$O/ H$_2$	Treatment length (h)	Spectral contribution SPM metallic cobalt (%)		
			CoPt/ SiO$_2$	CoMn (0.1)Pt/ SiO$_2$	CoMn (0.2)Pt/ SiO$_2$
0	0	48	47	66	69
7.5	0.25	48	50	N/A	65
14	0.50	48	49	N/A	67
20	0.75	48	48	N/A	69
25	1.0	48	48	70	68
	1.0	120	46	69	67
57	1.0	48	40	51	60
	1.0	120	39	48	53
	1.0	264	37	46	44

Fig. 5. *In situ* Mössbauer spectra of the Co(Mn)Pt/SiO$_2$ catalysts under FTS conditions at a relative humidity of (a) 25% and (b) 57%. The black lines represent the experimental spectra, the blue ones the fitted bulk metallic cobalt sextuplet, the red ones the small SPM metallic cobalt singlet, the orange ones the cobalt carbide doublet, and the purple ones the fitted oxidic cobalt doublet. (For interpretation of the references to colour in this figure legend, the reader is referred to the web version of this article.)

noted before that small metallic particles are more prone to oxidation and formation of MSCs [11,16,62]. The slight difference in the amount of cobalt silicate between the two manganese-promoted catalysts cannot be due to differences in the particle size. These two catalysts contain nearly similarly sized cobalt particles, following the similar initial SPM/sextuplet ratio and TEM imaging. Instead, the difference seems to stem from the rate at which cobalt silicate is formed. As the Mössbauer spectra are measured continuously over 11 days at an RH of 57 %, we can follow the formation of the different phases in time. Table 2 shows that the SPM contribution declines faster in the CoMn(0.1)Pt/SiO$_2$ catalyst, dropping to 51 % after 48 h compared to 60 % after 48 h for CoMn(0.2)Pt/SiO$_2$. This decline in SPM content is paired with the formation of cobalt-silicate, which contributed 25 % after 48 h for the CoMn(0.1)Pt/SiO$_2$ catalyst and only 7 % after 48 h for the CoMn(0.2)Pt/SiO$_2$ sample. The spectra recorded in inert following the high humidity test do not show significant differences anymore, with cobalt-silicate contributions of 33 % and 31 % for CoMn(0.1)Pt/SiO$_2$ and CoMn(0.2)Pt/SiO$_2$ respectively (Tables S3 and S4). This means that the amount of cobalt-silicate formed is very similar for both promoted catalyst samples, although it differs from the non-promoted sample. The formation of the cobalt-silicate phase has concurrently led to a decrease in the SPM to sextuplet ratio, as seen in Table 2. This indicates that smaller cobalt particles are more prone to forming MSCs. Thus, although manganese enhances cobalt dispersion, this also leads to a more extensive cobalt-silica interface, which can convert to inactive compounds under highly humid conditions.

3.4. Characterization of used catalysts

The non-radioactive samples in the Mössbauer cell during the consecutive humid FTS treatments were retrieved and further characterized. Representative TEM images of these catalysts are given in Fig. 6. Next to the cobalt nanoparticles, the images show the typical microstructure of cobalt-silicate compounds as fibrous strands covering the silica surface. In agreement with the *in situ* Mössbauer findings, the manganese-promoted samples contain more cobalt-silicate structures. Contrary to the previous study on a carbon support [24], no large agglomerates of manganese oxide are observed for the used catalysts by TEM. This shows that the promoter is still well dispersed over the silica support. The high contrast between the cobalt particles and the support highlights their metallic nature, their surface being passivated by wax or a thin oxide layer. However, we cannot exclude the possibility that manganese and cobalt are part of a mixed metal oxide, as was previously observed on a titania support [63]. The average size of the spherical cobalt nanoparticles was determined from these TEM images. As such, it was found that the average particle sizes are 9.9 ± 5.2 nm for Co/SiO$_2$, 7.2 ± 3.8 nm for CoMn(0.1)Pt/SiO$_2$, and 7.7 ± 5.4 nm for CoMn(0.2)Pt/SiO$_2$. Comparison of these results to the size of the oxidic precursor particles (Table 1) points to some sintering of the cobalt particles during the humid FTS treatments. The observation that sintering is most severe for the unpromoted catalyst confirms that manganese helps stabilize the dispersion of the cobalt nanoparticles in the silica-supported catalyst. Nevertheless, as discussed above and evident from the TEM images, the higher cobalt dispersion in the presence of manganese leads to a stronger propensity towards forming cobalt-silicate compounds under humid FTS conditions.

3.5. Catalytic activity

The catalytic performance of CoPt/SiO$_2$ and CoMn(0.1)Pt/SiO$_2$ as measured on-stream during the Mössbauer measurements is given in Fig. 7. Due to a technical issue with the TCD of the analysis equipment, the *in situ* activity of the CoMn(0.2)Pt/SiO$_2$ sample could not be measured. The CO conversion of CoPt/SiO$_2$ and CoMn(0.1)Pt/SiO$_2$ decreases with increasing RH of the feed. This is typical behavior for cobalt FTS catalysts, although the opposite has been reported [64,65]. At short time scales, the beneficial kinetic impact of water on the FT conversion can be more substantial than the deactivation, leading to a net increase in the FTS activity [66]. We also mention that the introduction of steam to the reactor feed results in a slight decrease of the CO and H$_2$ partial pressures, which can affect the catalytic activity due to the negative reaction order in CO and positive order in H$_2$ [67,68]. These aspects render a detailed discussion of the catalytic performance challenging. Accordingly, we focus here on the main trends. The decline in activity between RH = 0 % and 7.5 % for the non-promoted catalyst is much steeper than the decline for the manganese-promoted sample. Mössbauer spectra do not show substantial changes for both samples upon increasing the RH to 7.5 %, with the SPM content and the total metallic cobalt contribution remaining unchanged. Therefore, the initial activity loss might be a kinetic effect, such as competitive adsorption of oxygen-containing species at the higher steam partial pressure. Such an effect can be offset by the presence of manganese in the promoted catalyst, as it has been shown that manganese promotion can also increase the rate of CO dissociation [49,69]. Besides this initial difference, nevertheless, both catalysts show a gradual decline in activity at the higher humidity treatments, which can be correlated to a gradual transformation of the active cobalt phase into larger cobalt particles and the formation of less active cobalt carbide and cobalt silicate. While the promoted catalyst shows a significantly larger fraction of cobalt silicates, its activity is still higher than that of the non-promoted sample. TEM analysis of the used sample showed less sintering of the metallic cobalt phase in the promoted catalysts with an average particle size closer to the optimum size of 6 nm. So, the improved activity of the promoted catalyst is likely the result of the strong cobalt particle size
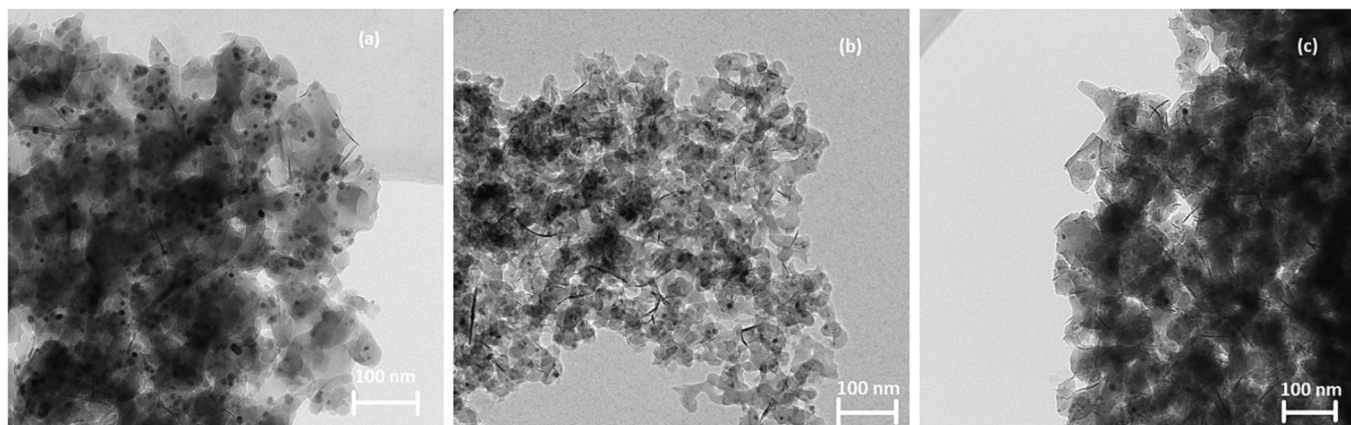

Fig. 6. Representative TEM images of used (a) CoPt/SiO$_2$, (b) CoMn(0.1)Pt/SiO$_2$ and (c) CoMn(0.2)Pt/SiO$_2$ following humid FTS treatments.
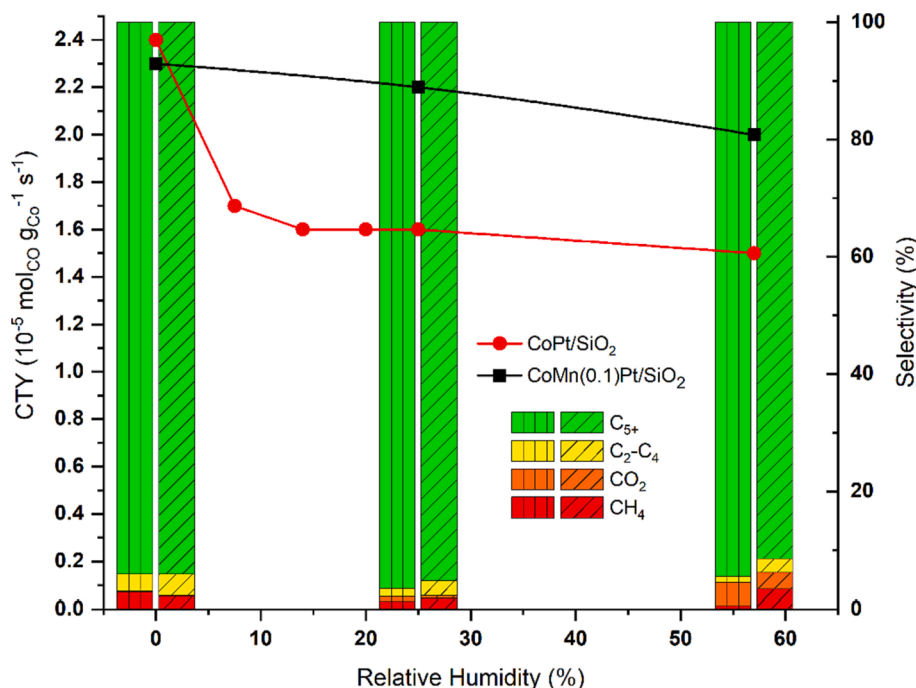
Fig. 7. Catalytic FTS performance at 200 °C, 20 bar pressure, $H_2/CO = 4$ as a function of the relative humidity in terms of CTY and the product distribution recorded in the Mössbauer cell for CoPt/SiO$_2$ (red dots) and CoMn(0.1)Pt/SiO$_2$ (black squares). The carbon-based selectivity is indicated by the bars for CoPt/SiO$_2$ (vertical line pattern) and CoMn(0.1)Pt/SiO$_2$ (diagonal line pattern). (For interpretation of the references to colour in this figure legend, the reader is referred to the web version of this article.)

effect as well as the promotional effect of the promoter itself, confirming the promising role of manganese as a promoter [4]. The product distribution during these *in situ* Mössbauer measurements does not change much with the RH, except for the apparent increased CO$_2$ selectivity at the highest RH of 57 %. This is most likely due to a more significant contribution of the water–gas shift reaction at high partial pressures of steam. Unlike the non-promoted catalyst, the CoMn(0.1)Pt/SiO$_2$ catalyst shows a slightly higher methane selectivity at the expense of C$_{5+}$ products at the highest RH. High steam partial pressures were achieved by removing the inert (Table S1), which also led to an increase in the CO and H$_2$ hydrogen partial pressures. This can explain the change in the product distribution. For instance, a higher CO partial pressure combined with a manganese oxide promoter resulted in more C$_1$ and C$_2$-C$_4$ products at the expense of C$_{5+}$ products [23]. Such an effect of high steam partial pressure on the product distribution was not observed for the non-promoted catalyst.

Besides the catalytic activity measurements in the *in situ* MES cell, the performance of the silica-supported cobalt catalysts was measured in a high-pressure fixed-bed plug-flow reactor at a temperature of 220 °C, a pressure of 20 bar, an H$_2$/CO ratio of 4, and a space velocity of 60 L g$_{cat}^{-1}$h^{-1}. The corresponding results for fresh and used catalysts are given in Table 3. The turnover frequencies (TOFs) of the catalysts are in the $2.8–6.4 \times 10^{-3}$ s^{-1} range, comparable to TOF values we previously found for cobalt on a carbon support [24]. They also are within the general range of TOFs observed during investigations of the particle size effect for cobalt catalysts [3–4]. The activity normalized on the amount of cobalt (CTY) shows a clear impact of manganese promotion, which was not observed in the Mössbauer experiments: the promoted samples are significantly less active than their non-promoted counterpart under these more representative test conditions. The observed average particle sizes for the two promoted catalysts in Table 1 are slightly below the optimum size of 6 nm [4]. As such, a slightly lower activity is to be expected for these samples. As the decrease in activity is much more pronounced, we attribute this to overpromotion with manganese, where a substantial part of the cobalt surface is covered by manganese oxide.

Table 3
Catalytic performance data for the cobalt catalysts (plug-flow reactor operated at 220 °C, 20 bar and H$_2$/CO = 4, SV = 60 L g$_{cat}^{-1}$h^{-1}).

Catalyst	Conversion (%)	C_1 sel. (%)	C_2-C_4 sel. (%)	C_{5+} sel. (%)	CTY (10^{-5} mol_{CO} g_{Co}^{-1} s^{-1})	TOF[a] (10^{-3} s^{-1})
CoPt/SiO$_2$	10	7	9	84	2.6	6.4
CoPt/SiO$_2$ used	2	5	6	89	0.75	3.0
CoMn(0.2) Pt/SiO$_2$	7	6	15	79	1.7	3.6
CoMn(0.2) Pt/SiO$_2$ used	3	12	3	85	1.0	3.1
CoMn(0.1) Pt/SiO$_2$	5	10	25	65	1.3	2.8

[a] TOF was based on the dispersion of TEM ($d_{p,Co} = (3/4) * d_{p,Co3O4}$), assuming spherical particles, full accessibility, and equal amounts of hcp and fcc cobalt.

Previously, it was found that manganese to cobalt ratio of 0.1 already led to a significant decrease in the FTS activity of a carbon nanofiber (CNF) supported cobalt catalyst [23]. The adverse effect of overpromotion seems stronger for the silica-supported case, possibly due to the increased stability of manganese oxide. Compared to silica, manganese was highly mobile on the CNF support [24]. Besides the decreased CTY values, the promoted catalysts show a significant increase in the C$_2$-C$_4$ selectivity. This shift in selectivity has been previously reported for catalysts overpromoted with manganese oxide, where the strong interaction between cobalt and manganese in the oxidic precursor was emphasized [23]. Concurrent work by Kimpel et al. [51] has shown that manganese promotion leads to a lower chain-growth probability when operating the reaction at high pressure. They show that CO dissociation is enhanced by the manganese promoter, which was also recently reported by Gupta et al. [70]. They propose that high carbon coverage results in a migration hindrance towards the step sites, which are highly

active for C–C coupling.

From a comparison of the catalytic performance in the fresh and used state, it is clear that the catalysts were significantly deactivated during the exposure to the various humid FTS treatments. The loss in CTY is more substantial for the non-promoted CoPt/SiO$_2$ catalyst. This is to be expected, as TEM showed more substantial sintering of cobalt, besides the formation of cobalt silicates. The less significant activity loss for the manganese-promoted CoMn(0.2)Pt/SiO$_2$ catalyst is in line with the less severe sintering of the metallic cobalt phase, which can be attributed to the structural promotion of manganese.

However, a more significant contribution of cobalt silicates was observed for the promoted catalyst. So, while the seemingly dominant deactivation due to sintering is likely less pronounced, additional deactivation occurs by forming such inactive cobalt silicates. This deactivation goes in parallel with a shift in the product distribution, with much of the selectivity towards C$_2$-C$_4$ products being lost in favor of methane and C$_{5+}$ products. This could result from the increasing average particle size, as larger particles favor C$_{5+}$ selectivity. However, like the FTS activity measured in the Mössbauer cell at high humidity, an increase in methane selectivity is also observed, suggesting smaller metallic particles. So, instead, the selectivity shift could come from manganese oxide promotion being less pronounced in the spent catalyst. Such a shift was also observed in a previous study, where during prolonged time on stream, the selectivity towards C$_1$ increased at the expense of C$_2$-C$_4$ products [71]. This is expected to result from manganese mobility under reaction conditions as it migrates from the metal onto the support, weakening the promotion effect. As a result, the used catalyst benefits from reduced manganese overpromotion compared to the fresh sample, which can explain the lower selectivity towards C$_2$-C$_4$ products.

4. Conclusions

The effect of humidity during FTS conditions, representing high CO conversion conditions, on manganese-promoted cobalt supported by silica was investigated by Mössbauer spectroscopy, TEM, and XPS. Promotion with manganese leads to a higher dispersion of the metallic cobalt particles in the reduced catalysts than in the unpromoted catalyst. *In situ* Mössbauer spectroscopy demonstrated that the enhanced dispersion of cobalt due to manganese promotion leads to more intimate contact with the support, resulting in cobalt silicates at elevated relative humidity that are inactive for the FTS reaction. In the absence of manganese, carbidization of relatively large particles was observed as a possible deactivation mechanism under high relative humidity conditions. The metallic cobalt phase in the used catalysts (having undergone *in situ* Mössbauer spectroscopy from low to high relative humidity) has a significantly lower dispersion than the metallic phase in the freshly reduced state. Sintering is more pronounced in the absence of manganese oxide, demonstrating the beneficial role of manganese as a structural promoter in cobalt-based FTS catalysts. Despite this, catalysts without and with manganese suffered from severe deactivation upon exposure to high partial pressures of steam due to the formation of less active cobalt phases. These findings highlight that silica is not a suitable support material for practical Fischer-Tropsch synthesis at bottom bed conditions with high CO conversion. Under mild conditions, however, the silica-supported cobalt exhibits excellent stability.

Declaration of Competing Interest

The authors declare that they have no known competing financial interests or personal relationships that could have appeared to influence the work reported in this paper.

Data availability

Data will be made available on request.

Appendix A. Supplementary data

Experimental conditions, Mössbauer fit parameters, manganese XPS spectra.

Supplementary data to this article can be found online at https://doi.org/10.1016/j.jcat.2023.115173.

References

[1] E. Iglesia, Design, synthesis, and use of cobalt-based Fischer-Tropsch synthesis catalysts, Appl. Catal. A 161 (1–2) (1997) 59–78, https://doi.org/10.1016/S0926-860X(97)00186-5.

[2] E. Rytter, N.E. Tsakoumis, A. Holmen, On the selectivity to higher hydrocarbons in Co-based Fischer-Tropsch synthesis, Catal. Today 261 (2016) 3–16, https://doi.org/10.1016/j.cattod.2015.09.020.

[3] J.P. den Breejen, P.B. Radstake, G.L. Bezemer, J.H. Bitter, V. Frøseth, A. Holmen, K.P. de Jong, On the origin of the cobalt particle size effects in Fischer–Tropsch catalysis, J. Am. Chem. Soc. 131 (20) (May 2009) 7197–7203, https://doi.org/10.1021/ja901006x.

[4] G.L. Bezemer, J.H. Bitter, H.P.C.E. Kuipers, H. Oosterbeek, J.E. Holewijn, X. Xu, F. Kapteijn, A.J. van Dillen, K.P. de Jong, Cobalt particle size effects in the Fischer–Tropsch reaction studied with carbon nanofiber supported catalysts, J. Am. Chem. Soc. 128 (12) (Mar. 2006) 3956–3964, https://doi.org/10.1021/ja058282w.

[5] N.E. Tsakoumis, M. Rønning, Ø. Borg, E. Rytter, A. Holmen, Deactivation of cobalt based Fischer-Tropsch catalysts: a review, Catal. Today 154 (3–4) (2010) 162–182, https://doi.org/10.1016/j.cattod.2010.02.077.

[6] P.J. van Berge, R.C. Everson, Cobalt as an alternative Fischer-Tropsch catalyst to iron for the production of middle distillates, Stud. Surf. Sci. Catal. 107 (15) (1997) 207–212, https://doi.org/10.1016/S0167-2991(97)80336-9.

[7] D. Moodley, M. Claeys, E. van Steen, P. van Helden, D. Kistamurthy, K.-J. Weststrate, H. Niemantsverdriet, A. Saib, W. Erasmus, J. van Loosdrecht, Sintering of cobalt during FTS: insights from industrial and model systems, Catal. Today 342 (Feb. 2020) 59–70, https://doi.org/10.1016/j.cattod.2019.03.059.

[8] E. Rytter, A. Holmen, Deactivation and regeneration of commercial type Fischer-Tropsch co-catalysts—a mini-review, Catalysts 5 (2) (Mar. 2015) 478–499, https://doi.org/10.3390/catal5020478.

[9] Z. Yu, Ø. Borg, D. Chen, E. Rytter, A. Holmen, Role of surface oxygen in the preparation and deactivation of carbon nanofiber supported cobalt Fischer-Tropsch catalysts, Top. Catal. 45 (1–4) (Aug. 2007) 69–74, https://doi.org/10.1007/s11244-007-0242-7.

[10] M. Wolf, B.K. Mutuma, N.J. Coville, N. Fischer, M. Claeys, Role of CO in the water-induced formation of cobalt oxide in a high conversion Fischer-Tropsch environment, ACS Catal. 8 (5) (May 2018) 3985–3989, https://doi.org/10.1021/acscatal.7b04177.

[11] E. Van Steen, M. Claeys, M.E. Dry, J. Van De Loosdrecht, E.L. Viljoen, J.L. Visagie, Stability of nanocrystals: thermodynamic analysis of oxidation and re-reduction of cobalt in water/hydrogen mixtures, J. Phys. Chem. B 109 (8) (2005) 3575–3577, https://doi.org/10.1021/jp045136o.

[12] P.J. Van Berge, J. Van De Loosdrecht, S. Barradas, A.M. Van Der Kraan, Oxidation of cobalt based Fischer-Tropsch catalysts as a deactivation mechanism, Catal. Today 58 (4) (2000) 321–334, https://doi.org/10.1016/S0920-5861(00)00265-0.

[13] J. van de Loosdrecht, B. Balzhinimaev, J.A. Dalmon, J.W. Niemantsverdriet, S.V. Tsybulya, A.M. Saib, P.J. van Berge, J.L. Visagie, Cobalt Fischer-Tropsch synthesis: deactivation by oxidation? Catal. Today 123 (1–4) (2007) 293–302, https://doi.org/10.1016/j.cattod.2007.02.032.

[14] W. Zhou, J.-G. Chen, K.-G. Fang, Y.-H. Sun, The deactivation of Co/SiO$_2$ catalyst for Fischer-Tropsch synthesis at different ratios of H$_2$ to CO, Fuel Process. Technol. 87 (7) (Jul. 2006) 609–616, https://doi.org/10.1016/j.fuproc.2006.01.008.

[15] G. Prieto, A. Martínez, P. Concepción, R. Moreno-Tost, Cobalt particle size effects in Fischer-Tropsch synthesis: structural and in situ spectroscopic characterisation on reverse micelle-synthesised Co/ITQ-2 model catalysts, J. Catal. 266 (1) (Aug. 2009) 129–144, https://doi.org/10.1016/j.jcat.2009.06.001.

[16] M. Wolf, E.K. Gibson, E.J. Olivier, J.H. Neethling, C.R.A. Catlow, N. Fischer, M. Claeys, In-depth characterisation of metal-support compounds in spent Co/SiO$_2$ Fischer-Tropsch model catalysts, Catal. Today 342 (Feb. 2020) 71–78, https://doi.org/10.1016/j.cattod.2019.01.065.

[17] C.H. Bartholomew, Mechanisms of catalyst deactivation, Appl. Catal. A 212 (1–2) (Apr. 2001) 17–60, https://doi.org/10.1016/S0926-860X(00)00843-7.

[18] M. Sadeqzadeh, S. Chambrey, J. Hong, P. Fongarland, F. Luck, D. Curulla-Ferré, D. Schweich, J. Bousquet, A.Y. Khodakov, Effect of different reaction conditions on the deactivation of alumina-supported cobalt Fischer-Tropsch catalysts in a milli-fixed-bed reactor: Experiments and modeling, Ind. Eng. Chem. Res. 53 (17) (2014) 6913–6922, https://doi.org/10.1021/ie4040303.

[19] A.M. Saib, D.J. Moodley, I.M. Ciobîcă, M.M. Hauman, B.H. Sigwebela, C.J. Weststrate, J.W. Niemantsverdriet, J. Van De Loosdrecht, Fundamental understanding of deactivation and regeneration of cobalt Fischer-Tropsch synthesis

catalysts, Catal. Today 154 (3–4) (2010) 271–282, https://doi.org/10.1016/j.cattod.2010.02.008.

[20] M. Rahmati, M.S. Safdari, T.H. Fletcher, M.D. Argyle, C.H. Bartholomew, Chemical and thermal sintering of supported metals with emphasis on cobalt catalysts during Fischer-Tropsch synthesis, Chem. Rev. 120(10) (May 27, 2020) 4455–4533, 10.1021/acs.chemrev.9b00417.

[21] M. Claeys, M.E. Dry, E. van Steen, P.J. van Berge, S. Booyens, R. Crous, P. van Helden, J. Labuschagne, D.J. Moodley, A.M. Saib, Impact of process conditions on the sintering behavior of an alumina-supported cobalt Fischer-Tropsch catalyst studied with an in situ magnetometer, ACS Catal. 5 (2) (Feb. 2015) 841–852, https://doi.org/10.1021/cs501810y.

[22] M.D. Argyle, T.S. Frost, C.H. Bartholomew, Cobalt fischer-tropsch catalyst deactivation modeled using generalized power law expressions, Top. Catal. 57 (6–9) (2014) 415–429, https://doi.org/10.1007/s11244-013-0197-9.

[23] G.L. Bezemer, P. Radstake, U. Falke, H. Oosterbeek, H. Kuipers, A. Van Dillen, K. De Jong, Investigation of promoter effects of manganese oxide on carbon nanofiber-supported cobalt catalysts for Fischer-Tropsch synthesis, J. Catal. 237 (1) (Jan. 2006) 152–161, https://doi.org/10.1016/j.jcat.2005.10.031.

[24] L. M. van Koppen, A. Iulian Dugulan, G. Leendert Bezemer, E. J. M. Hensen, Sintering and carbidization under simulated high conversion on a cobalt-based Fischer-Tropsch catalyst; manganese oxide as a structural promotor, J. Catal. 413 (Sep. 2022) 106–118, 10.1016/j.jcat.2022.06.020.

[25] A. Carvalho, V.V. Ordomsky, Y. Luo, M. Marinova, A.R. Muniz, N.R. Marcilio, A. Y. Khodakov, Elucidation of deactivation phenomena in cobalt catalyst for Fischer-Tropsch synthesis using SSITKA, J. Catal. 344 (2016) 669–679, https://doi.org/10.1016/j.jcat.2016.11.001.

[26] B. Ernst, S. Libs, P. Chaumette, A. Kiennemann, Preparation and characterization of Fischer-Tropsch active Co/SiO2 catalysts, Appl. Catal. A 186 (1–2) (1999) 145–168, https://doi.org/10.1016/S0926-860X(99)00170-2.

[27] H. Karaca, J. Hong, P. Fongarland, P. Roussel, A. Griboval-Constant, M. Lacroix, K. Hortmann, O.V. Safonova, A.Y. Khodakov, In situ XRD investigation of the evolution of alumina-supported cobaltcatalysts under realistic conditions of Fischer-Tropsch synthesis, Chem. Commun. 46 (5) (2010) 788–790, https://doi.org/10.1039/B920110F.

[28] A. Rochet, V. Moizan, F. Diehl, C. Pichon, V. Briois, Quick-XAS and Raman operando characterisation of a cobalt alumina-supported catalyst under realistic Fischer-Tropsch reaction conditions, Catal. Today 205 (2013) 94–100, https://doi.org/10.1016/j.cattod.2012.08.021.

[29] T.O. Eschemann, K.P. de Jong, Deactivation Behavior of Co/TiO2 Catalysts during Fischer-Tropsch Synthesis, ACS Catal. 5 (6) (Jun. 2015) 3181–3188, https://doi.org/10.1021/acscatal.5b00268.

[30] T.O. Eschemann, J.H. Bitter, K.P. De Jong, Effects of loading and synthesis method of titania-supported cobalt catalysts for Fischer-Tropsch synthesis, Catal. Today 228 (2014) 89–95, https://doi.org/10.1016/j.cattod.2013.10.041.

[31] C.E. Kliewer, S.L. Soled, G. Kiss, Morphological transformations during Fischer-Tropsch synthesis on a titania-supported cobalt catalyst, Catal. Today 323 (Feb. 2019) 233–256, https://doi.org/10.1016/j.cattod.2018.05.021.

[32] M. Mehrbod, M. Martinelli, A.G. Martino, D.C. Cronauer, A. Jeremy Kropf, C. L. Marshall, G. Jacobs, Fischer-Tropsch synthesis: direct cobalt nitrate reduction of promoted Co/TiO2 catalysts, Fuel 245 (February) (Jun. 2019) 488–504, https://doi.org/10.1016/j.fuel.2019.02.083.

[33] S.J. Tauster, S.C. Fung, R.L. Garten, Strong metal-support interactions. Group 8 noble metals supported on titanium dioxide, J. Am. Chem. Soc. 100 (1) (Jan. 1978) 170–175, https://doi.org/10.1021/ja00469a029.

[34] S.J. Tauster, S.C. Fung, R.T.K. Baker, J.A. Horsley, Strong interactions in supported-metal catalysts, Science (1979) 211(4487) (Mar. 1981) 1121–1125, 10.1126/science.211.4487.1121.

[35] M. Wolf, E.K. Gibson, E.J. Olivier, J.H. Neethling, C.R.A. Catlow, N. Fischer, M. Claeys, Water-induced formation of cobalt-support compounds under simulated high conversion Fischer-Tropsch environment, ACS Catal. 9 (6) (Jun. 2019) 4902–4918, https://doi.org/10.1021/acscatal.9b00160.

[36] M. Wolf, N. Fischer, M. Claeys, Water-induced deactivation of cobalt-based Fischer-Tropsch catalysts, Nat. Catal. 3 (12) (Dec. 2020) 962–965, https://doi.org/10.1038/s41929-020-00534-5.

[37] H. Karaca, O.V. Safonova, S. Chambrey, P. Fongarland, P. Roussel, A. Griboval-Constant, M. Lacroix, A.Y. Khodakov, Structure and catalytic performance of Pt-promoted alumina-supported cobalt catalysts under realistic conditions of Fischer-Tropsch synthesis, J. Catal. 277 (1) (Jan. 2011) 14–26, https://doi.org/10.1016/j.jcat.2010.10.007.

[38] G.L. Bezemer, T.J. Remans, A.P. van Bavel, A.I. Dugulan, Direct evidence of water-assisted sintering of cobalt on carbon nanofiber catalysts during simulated Fischer–Tropsch conditions revealed with in situ Mössbauer spectroscopy, J. Am. Chem. Soc. 132 (25) (Jun. 2010) 8540–8541, https://doi.org/10.1021/ja103002k.

[39] M. Claeys, M.E. Dry, E. van Steen, E. du Plessis, P.J. van Berge, A.M. Saib, D. J. Moodley, In situ magnetometer study on the formation and stability of cobalt carbide in Fischer-Tropsch synthesis, J. Catal. 318 (Oct. 2014) 193–202, https://doi.org/10.1016/j.jcat.2014.08.002.

[40] T. Lin, K. Gong, C. Wang, Y. An, X. Wang, X. Qi, S. Li, Y. Lu, L. Zhong, Y. Sun, Fischer-Tropsch synthesis to olefins: catalytic performance and structure evolution of Co2C-based catalysts under a CO2 environment, ACS Catal. 9 (10) (2019) 9554–9567, https://doi.org/10.1021/acscatal.9b02513.

[41] Z. Li, L. Zhong, F. Yu, Y. An, Y. Dai, Y. Yang, T. Lin, S. Li, H. Wang, P. Gao, Y. Sun, M. He, Effects of sodium on the catalytic performance of CoMn catalysts for Fischer-Tropsch to Olefin reactions, ACS Catal. 7 (5) (May 2017) 3622–3631, https://doi.org/10.1021/acscatal.6b03478.

[42] X. Wang, W. Chen, T. Lin, J. Li, F. Yu, Y. An, Y. Dai, H. Wang, L. Zhong, Y. Sun, Effect of the support on cobalt carbide catalysts for sustainable production of olefins from syngas, Cuihua Xuebao/Chinese J. Catal. 39 (12) (2018) 1869–1880, https://doi.org/10.1016/S1872-2067(18)63153-5.

[43] H. Storch, The Fischer-Tropsch and Related Processes for Synthesis of Hydrocarbons by Hydrogenation of Carbon Monoxide, Wiley, New York, 1948, pp. 115–156. 10.1016/S0360-0564(08)60674-4.

[44] M. van der Riet, G.J. Hutchings, R.G. Copperthwaite, Selective formation of C3 hydrocarbons from CO + H2 using cobalt–manganese oxide catalysts, J. Chem. Soc. Chem. Commun. no. 10 (1986) 798–799, https://doi.org/10.1039/C39860000798.

[45] S. Colley, R.G. Copperthwaite, G.J. Hutchings, M. Van der Riet, Carbon monoxide hydrogenation using cobalt manganese oxide catalysts: initial catalyst optimization studies, Ind. Eng. Chem. Res. 27 (8) (Aug. 1988) 1339–1344, https://doi.org/10.1021/ie00080a001.

[46] G. J. Hutchings, M. van der Riet, R. Hunter, CO hydrogenation using cobalt/manganese oxide catalysts. Comments on the mechanism of carbon–carbon bond formation, J. Chem. Soc., Faraday Trans. 1: Phys. Chem. Condensed Phases 85(9) (1989) 2875, 10.1039/f19898502875.

[47] S.E. Colley, R.G. Copperthwaite, G.J. Hutchings, S.P. Terblanche, M.M. Thackeray, Identification of body-centred cubic cobalt and its importance in CO hydrogenation, Nature 339 (6220) (May 1989) 129–130, https://doi.org/10.1038/339129a0.

[48] F. Morales, F.M.F. De Groot, P. Glatzel, E. Kleimenov, H. Bluhm, M. Hävecker, A. Knop-Gericke, B.M. Weckhuysen, In situ X-ray absorption of Co/Mn/TiO2 catalysts for fischer-tropsch synthesis, J. Phys. Chem. B 108 (41) (2004) 16201–16207, https://doi.org/10.1021/jp0403846.

[49] F. Morales, F. De Groot, O. Gijzeman, A. Mens, O. Stephan, B. Weckhuysen, Mn promotion effects in Co/TiO2 Fischer-Tropsch catalysts as investigated by XPS and STEM-EELS, J. Catal. 230 (2) (Mar. 2005) 301–308, https://doi.org/10.1016/j.jcat.2004.11.047.

[50] A.Y. Khodakov, W. Chu, P. Fongarland, Advances in the development of novel cobalt Fischer-Tropsch catalysts for synthesis of long-chain hydrocarbons and clean fuels, Chem. Rev. 107 (5) (2007) 1692–1744, https://doi.org/10.1021/cr050972v.

[51] T.F. Kimpel, J.X. Liu, W. Chen, R. Pestman, E.J.M. Hensen, Pressure dependence and mechanism of Mn promotion in Co catalyzed Fischer-Tropsch reaction, J. Catal. 425 (2023) 181–195.

[52] M.W.J. Crajé, A.M. Van der Kraan, J. Van de Loosdrecht, P.J. Van Berge, The application of Mössbauer emission spectroscopy to industrial cobalt based Fischer-Tropsch catalysts, Catal. Today 71 (3–4) (2002) 369–379, https://doi.org/10.1016/S0920-5861(01)00464-3.

[53] L.M. van Koppen, A. Iulian Dugulan, G. Leendert Bezemer, E.J.M. Hensen, Elucidating deactivation of titania-supported cobalt Fischer-Tropsch catalysts under simulated high conversion conditions, J. Catal. 420 (Apr. 2023) 44–57, https://doi.org/10.1016/j.jcat.2023.02.019.

[54] M.C. Biesinger, B.P. Payne, A.P. Grosvenor, L.W.M. Lau, A.R. Gerson, R. St, C. Smart, Resolving surface chemical states in XPS analysis of first row transition metals, oxides and hydroxides: Cr, Mn, Fe, Co and Ni, Appl. Surf. Sci. 257 (7) (Jan. 2011) 2717–2730, https://doi.org/10.1016/j.apsusc.2010.10.051.

[55] Z. Klencsár, MossWinn—methodological advances in the field of Mössbauer data analysis, Hyperfine Interact. 217 (1–3) (Apr. 2013) 117–126, https://doi.org/10.1007/s10751-012-0732-2.

[56] J.A. Tjon, M. Blume, Mössbauer spectra in a fluctuating environment II. Randomly varying electric field gradients, Phys. Rev. 165 (2) (Jan. 1968) 456–461, https://doi.org/10.1103/PhysRev.165.456.

[57] P. Scherrer, Estimation of the size and internal structure of colloidal particles by means of Röntgen, Nachrichten Von Der Gesellschaft Der Wissenschaften Zu Göttingen 2 (1918) 96–100.

[58] T.W. van Deelen, J.J. Nijhuis, N.A. Krans, J. Zečević, K.P. de Jong, Preparation of cobalt nanocrystals supported on metal oxides to study particle growth in Fischer-Tropsch catalysts, ACS Catal. 8 (11) (Nov. 2018) 10581–10589, https://doi.org/10.1021/acscatal.8b03094.

[59] F. Morales, D. Grandjean, F.M.F. de Groot, O. Stephan, B.M. Weckhuysen, Combined EXAFS and STEM-EELS study of the electronic state and location of Mn as promoter in Co-based Fischer-Tropsch catalysts, PCCP 7 (4) (2005) 568–572, https://doi.org/10.1039/B418286C.

[60] G.M. Bancroft, A.G. Maddock, R.G. Burns, Applications of the Mössbauer effect to silicate mineralogy—I. Iron silicates of known crystal structure, Geochim. Cosmochim. Acta 31 (11) (Nov. 1967) 2219–2246, https://doi.org/10.1016/0016-7037(67)90062-2.

[61] L.C. Browning, P.H. Emmett, Equilibrium measurements in the Ni3C-Ni-CH4-H2 and Co2C-Co-CH4-H2 systems, J. Am. Chem. Soc. 74 (7) (Apr. 1952) 1680–1682, https://doi.org/10.1021/ja01127a021.

[62] M. Wolf, H. Kotzé, N. Fischer, M. Claeys, Size dependent stability of cobalt nanoparticles on silica under high conversion Fischer-Tropsch environment, Faraday Discuss. 197 (2017) 243–268, https://doi.org/10.1039/C6FD00200E.

[63] F. Morales, D. Grandjean, A. Mens, F.M.F. de Groot, B.M. Weckhuysen, X-ray absorption spectroscopy of Mn/Co/TiO2 Fischer–Tropsch catalysts: relationships between preparation method, molecular structure, and catalyst performance, J. Phys. Chem. B 110 (17) (May 2006) 8626–8639, https://doi.org/10.1021/jp0565958.

[64] E. Rytter, Ø. Borg, N.E. Tsakoumis, A. Holmen, Water as key to activity and selectivity in Co Fischer-Tropsch synthesis: γ-alumina based structure-performance relationships, J. Catal. 365 (2018) 334–343, https://doi.org/10.1016/j.jcat.2018.07.003.

[65] E. Rytter, A. Holmen, Perspectives on the effect of water in cobalt Fischer-Tropsch synthesis, ACS Catal. 7 (8) (2017) 5321–5328, https://doi.org/10.1021/acscatal.7b01525.

[66] Ø. Borg, Z. Yu, D. Chen, E.A. Blekkan, E. Rytter, A. Holmen, The effect of water on the activity and selectivity for carbon nanofiber supported cobalt fischer-tropsch catalysts, Top. Catal. 57 (6–9) (2014) 491–499, https://doi.org/10.1007/s11244-013-0205-0.

[67] W. Chen, R. Pestman, B. Zijlstra, I.A.W. Filot, E.J.M. Hensen, Mechanism of cobalt-catalyzed CO hydrogenation: 1. Methanation, ACS Catal. 7 (12) (Dec. 2017) 8050–8060, https://doi.org/10.1021/acscatal.7b02757.

[68] R. Pestman, W. Chen, E. Hensen, Insight into the rate-determining step and active sites in the Fischer-Tropsch Reaction over cobalt catalysts, ACS Catal. 9 (5) (May 2019) 4189–4195, https://doi.org/10.1021/acscatal.9b00185.

[69] F. Morales, E. de Smit, F. de Groot, T. Visser, B. Weckhuysen, Effects of manganese oxide promoter on the CO and H_2 adsorption properties of titania-supported cobalt Fischer-Tropsch catalysts, J. Catal. 246 (1) (Feb. 2007) 91–99, https://doi.org/10.1016/j.jcat.2006.11.014.

[70] S.S. Gupta, P.M. Shenai, J. Meeuwissen, G.L. Bezemer, S. Shetty, Electronic promotion effects of metal oxides: a case study of mnO impact on Fischer-Tropsch catalysis, J. Phys. Chem. C 125 (39) (Oct. 2021) 21390–21401, https://doi.org/10.1021/acs.jpcc.1c05278.

[71] M. van der Riet, R.G. Copperthwaite, G.J. Hutchings, Formation of hydrocarbons from CO + H_2 using a cobalt–manganese oxide catalyst. A ^{13}C isotopic study, J. Chem. Soc., Faraday Trans. 1: Phys. Chem. Condensed Phases 83(9) (1987) 2963, 10.1039/f19878302963.